Article

Effect of the Fe/Mn Ratio on the Microstructural Evolution of the AA6063 Alloy with Homogenization Heat Treatment Interruption

Adolfo Galván Avalos *, Jesús Torres Torres * and Alfredo Flores Valdés

Cinvestav Saltillo, Industria Metalúrgica 1062, Ramos Arizpe 25900, Mexico; alfredo.flores@cinvestav.edu.mx
* Correspondence: adolfo.galvan@cinvestav.mx (A.G.A.); jesus.torres@cinvestav.edu.mx (J.T.T.);
   Tel.: +52-844-243-4744 (A.G.A.); +52-844-438-9600 (J.T.T.)

Abstract: The casting structure of the AA6063 alloy contains intermetallic particles of β-Al_5FeSi, which can result in the fragility of the cast pieces. However, with heat treatment, the β phase transforms from a needle or plate form into an intermetallic phase known as α, which resembles Chinese-script in its morphology. To analyze the effect of the ratio of Fe/Mn with different ratios of 0.5, 0.75, and 1, a heat treatment process is used with intermittent interruptions. The alloy is subjected to a temperature of 575 °C for 12 h to determine the microstructural evolution of the β-Al_6FeMn and α-$Al_{15}(FeMn)_3Si_2$ phases. This study used scanning electron microscopy to conduct point analyses and elemental mappings of the intermetallics found in the casting and heat treatment samples. Additionally, X-ray diffraction was employed to determine the stoichiometry of the present phases. The results indicated that the cast structure contains β-Al_6FeMn and α-$Al_{15}(FeMn)_3Si_2$ phases and that the β-Al_6FeMn phase transforms into the α-$Al_{15}(FeMn)_3Si_2$ phase upon completion of the heat treatment process. By using specific Fe/Mn ratios, the formation of the needle-shaped Al_5FeSi phase in the casting structure of the alloy can be inhibited, leading to the precipitation of phases such as β-Al_6FeMn and α-$Al_{15}(FeMn)_3Si_2$ instead.

Keywords: heat treatment; AA6063 alloy; homogenization; mapping; Chinese-script morphology

1. Introduction

The aluminum alloy Al–Mg–Si is a combination of medium mechanical strength, good corrosion resistance, excellent formability, weldability, and easy recycling. The main alloying elements are Mg and Si, which provide heat treatment capabilities [1].

As a result, it is widely used to make large casts with sophisticated structures for the transportation industry, including chassis frames and battery module housings for electric cars [2]. The Al 6063 is known as a ternary Al–Mg–Si alloy; also, it can be considered a quaternary alloy since Fe is a controlled impurity. In the casting of primary or recycled aluminum alloys, Fe, Si, and Mg migrate to grain boundaries and interdendritic regions of the α-Al matrix during solidification. This promotes the formation of iron-enriched intermetallic compounds [3].

Iron levels ranging from 0.4 to 0.8% in recycled aluminum scrap can have a detrimental effect on the alloy's properties. This is particularly true for the formation of needle-shaped β-Al_5FeSi intermetallics during solidification, which can compromise mechanical properties, including ductility and fatigue strength. As such, careful attention is necessary to ensure that these high iron levels are appropriately managed to maintain the desired quality of the alloy [4,5].

Alloys containing Al–Mg–Si are not recommended for hot forming while in their cast state. This is due to the presence of particles, mainly consisting of β-Al_5FeSi, α-Al_8Fe_2Si, and Mg_2Si during solidification. Various factors such as alloy composition, cooling rate,

and Fe content influence the morphology of Fe-rich phases. As for the solidification process, α-Al$_8$Fe$_2$Si typically forms at higher cooling rates than β-Al$_5$FeSi [6].

The large size needle/platelet β-Al$_5$FeSi phase can induce severe casting defects and declined properties. The other kind of Fe-rich phase in Al–Mg–Si alloy is the α-AlFeSi phase, whose chemical formula is α-Al$_8$Fe$_2$Si (or α-Al$_{15}$Fe$_3$Si$_2$). Depending on the alloying elements and cooling conditions, the α-AlFeSi phase appears as hexagonal, star-like, dendritic, Chinese script, or globular shape. Hereinto, the needle-like β-AlFeSi phase deteriorates the mechanical properties since its sharp interfaces act as the location of high stress concentration. Conversely, the Chinese script-like α-AlFeSi phase is relatively harmless [7,8].

The homogenization process is critical for low-cost mechanical deformation without defects. It involves heat treatment to improve the quality of billets [9,10]. The heat treatment aims to dissolve particles of Mg$_2$Si and low-melting silicon, which cause cracking during the process. It also aims to obtain the phase transformation of β-Al$_5$FeSi to α-Al$_{12}$(FeMn)$_3$Si particles and spheroidize α particles, improving extrusion properties [11,12].

The process of homogenization treatment involves the formation of globular phases, reduction of segregation, and precipitation of dispersoids. In Al–Mn–Fe–Si (–Mg) alloys, the term dispersoid refers to intermetallic particles usually on a nanoscale level. The type of dispersoids formed in Al–Mn–Fe–Si alloys depends on the total quantity of Si present. For alloys with low Si content, the dispersoids are generally in the form of the plate-like Al$_6$FeMn phase, whereas, for alloys with high Si content, the dispersoids are in the cubic α-Al(FeMn)Si phase [13].

To reduce the fragility of the intermetallic compound β-AlFeSi, researchers have focused on changing the morphology of this phase. One method adds elements like Be, Mn, Cr, or V that promote dispersoid formation. Among these elements, manganese is the most efficient. Manganese acts as a catalyst and increases the phase transformation rate from β-AlFeSi to α-Al(FeMn)Si at high holding temperatures. The resulting α-Al(MnFe)Si phase has a body-centered cubic structure and is known for its Chinese-script morphology [14,15].

A study suggest that the stability zones of the αH-AlFeSi (hexagonal) and αc-AlFeMnSi (cubic) phases are limited to a concentration range where the weight of Mn is less than 0.5% [16].

Adding Mn to aluminum–silicon alloys increases the total number of intermetallic compounds containing (Fe + Mn), such as Al$_6$FeMn and AlFeMnSi. To promote the precipitation of the α-Fe phase, it is recommended to maintain an Fe/Mn ratio greater than 0.5 [17]. As a common alloying element, Mn has a relatively low cost and is generally used for alloy strengthening. Moreover, the addition of Mn can eliminate the β-AlFeSi phase and promote the formation of the α-Al(FeMn)Si phase, which is beneficial for the mechanical properties [18].

The solidification conditions and the presence of other elements such as Cu and Mg lessen the efficiency of Mn in aluminum–silicon alloys. However, the phase transformation from the β plate-like form to α with the Chinese-script form is not completely inhibited, even with a Mn/Fe ratio of up to 2. When the Mn/Fe ratio is around 1.2, the intermetallic phase β-Al$_5$FeSi is wholly converted to the α-Al$_{13}$(FeMn)$_4$Si$_2$ phase [19]. Table 1 shows the phases present in the 6XXX series [20].

A recent work reports the analysis of variables like that of this study, which are the effect of variations in the Mn/Cr ratios (0.5–8) on the precipitation behavior of dispersoids in 6XXX series aluminum alloys, with homogenization thermal treatment at different temperatures 500, 530, and 560 °C and residence times of 0–24 h [21]. Another study analyzed the individual and synergistic effects of Mn and Cu on the microstructure evolution and mechanical properties [22].

Table 1. Intermetallic phases in the 6xxx series.

Phase	Structure	Stoichiometry
$\alpha_c(\alpha)$AlFeSi	Cubic	$Al_{12}Fe_3Si$, $Al_{12-15}Fe_3Si_{1-2}$
	Cubic	$Al_{12}(FeMn)_3Si$, $Al_{15}(FeMn)_3Si_2$
	Cubic	$Al_{12}Mn_3Si$, $Al_{15}Mn_3Si_2$, Al_9Mn_2Si
$\alpha_h(\alpha')$-AlFeSi	hexagonal	Al_8Fe_2Si
β-AlFeSi	monoclinic	$Al_{4.5}FeSi$

The objective of this research is to analyze the impact of the Fe/Mn ratio on microstructural alterations that occur during homogenization heat treatment, specifically how this ratio influences the $\beta \rightarrow \alpha$ transformation and its behavior during mechanical forming. To evaluate the microstructural changes in the β and α phases, a homogenization heat treatment on the alloy using varying Fe/Mn ratios (0.5, 0.75, and 1) was performed and halted at a temperature of 575 °C for 12 h; the samples were cooled in water at room temperature every 30 min until we reached a total time of 660 min. Subsequently, we mechanically roughed the samples with SiC paper from #80 to #2400, polished them with 3 and 1 μm diamond paste, and finished them with 0.06 μm colloidal silica to attain a mirror-like finish. Lastly, we prepared the samples for microstructural analysis.

Scanning electron microscopy was used to conduct point analyses and elemental mappings of the intermetallic presents in the casting and heat treatment samples. Also, X-ray diffraction was utilized to determine the stoichiometry of the phases present. The results showed that the β-Al_6FeMn and α-$Al_{15}(FeMn)_3Si_2$ phases are in the cast structure and the phase β-Al_6FeMn is transformed into phase α-$Al_{15}(FeMn)_3Si_2$ when the heat treatment ends.

2. Materials and Methods

To manufacture preforms, the raw material (aluminum profile) is melted. The raw material needed to obtain the AA6063 alloy was prepared using aluminum profile scrap in a 50 kg silicon carbide crucible gas furnace. This process results in ingots with the same chemical composition. Table 2 shows the results obtained.

Table 2. Chemical composition of the ingots (%wt).

Si	Fe	Mn	Mg	Cu	Zn	Others	Al
0.55	0.237	0.014	0.23	0.03	0.02	0.019	Bal

An induction furnace with a capacity of 14 kg was used to obtain the preforms. The process consisted of melting the raw material to obtain liquid metal. Once this step was complete, the required amount of Fe determined for each of the Fe/Mn ratios was added in the form of a wire at 850 °C. A time of 1 h was provided to ensure its dissolution in the metal bath with mechanical agitation for 15 min. The next stage involved adding the determined amount of Mn flakes at 850 °C without mechanical agitation. Finally, argon gas was injected into the metal bath to degas for 10 min. The final stage involves the removal of the liquid metal. This was conducted at a temperature of 750 °C, using a steel mold preheated to 450 °C with a rectangular shape in a vertical position. The process was repeated for each Fe/Mn ratio used. The chemical composition of the alloys was determined by atomic emission spectroscopy. Table 3 shows the alloys' chemical composition and Fe/Mn ratios.

Table 3. The chemical composition (%wt) and Fe/Mn ratios of the alloys used in this study.

Fe/Mn	Si	Fe	Mn	Mg	Cu	Zn	Others	Al
1	0.55	0.7	0.7	0.23	0.3	0.02	0.019	Bal
0.75	0.55	0.6	0.8	0.23	0.3	0.02	0.019	Bal
0.5	0.55	0.55	1.1	0.23	0.3	0.02	0.019	Bal

The obtained preforms have dimensions of 381 mm length, 102 mm width, and 12.7 mm thickness. These preforms had a rectangular shape and underwent a homogenization heat treatment at a temperature of 575 °C for 11 h. A sample was obtained every 30 min until reaching 11 h. After the heat treatment, they were cooled in water at room temperature. This heat treatment aimed to analyze its effect on the precipitation of the phases β and α for each of the different Fe/Mn ratios.

The samples were sectioned and prepared for microstructural analysis by being first mechanically roughed with SiC paper from #80 to #2400. Then, they were polished with 3 and 1 μm diamond paste, and, finally, finished with a mirror-like finish using 0.06 μm colloidal silica.

The specimens underwent chemical exposure to the Keller reagent, which comprises 2 mL HF, 3 mL HCl, 5 mL HNO_3, and 190 mL H_2O. This reagent made it possible to expose the β and α phases, which are distinguished by distinct coloration. To assess the percentages of each phase present in each condition, for the Fe/Mn ratio and heat treatment time, Image-Pro 6.0 software was utilized. To capture measurements and quantify the phases, 10 field micrographs were taken of each sample using a Keyence optical microscope VHX-6000 (Keyence, Osaka, Japan) and Image-Pro Plus 6.0 software.

A JEOL model JSM-7800F PRIME scanning electron microscope (JEOL Ltd., Akijima, Japan) with a BRUKER QUANTAX EDS microanalysis system was used to obtain micrographs of cast and heat-treated samples after 660 min. The microstructure was analyzed to determine the presence and quantification of each element present in the intermetallic compounds of each sample. Elemental mappings were carried out to carry out this analysis. Additionally, BRUKER model D8 ADVANCE ECO X-ray diffraction equipment (Bruker, Billerica, MA, USA) was used to examine the samples. The results obtained were analyzed with Match! 3 software version 3.16 Build 288 to determine which phase corresponds to the intermetallics present in the microstructure. The Inorganic Crystal Structure Database (ICSD) and the Match! 3 software were used for the analysis of the diffraction patterns obtained from each of the samples.

3. Results and Discussion

3.1. Analysis of the Microstructure of the β and α Phases Using SEM

To understand how variables such as the duration of the homogenization heat treatment and the Fe/Mn (0.5, 0.75, and 1) ratios in the chemical composition affect microstructural changes in the samples, we conducted a punctual analysis and elemental mapping using scanning electron microscopy. Figure 1 shows micrographs taken at 500× magnification of the casts and homogenized samples that were treated for 660 min.
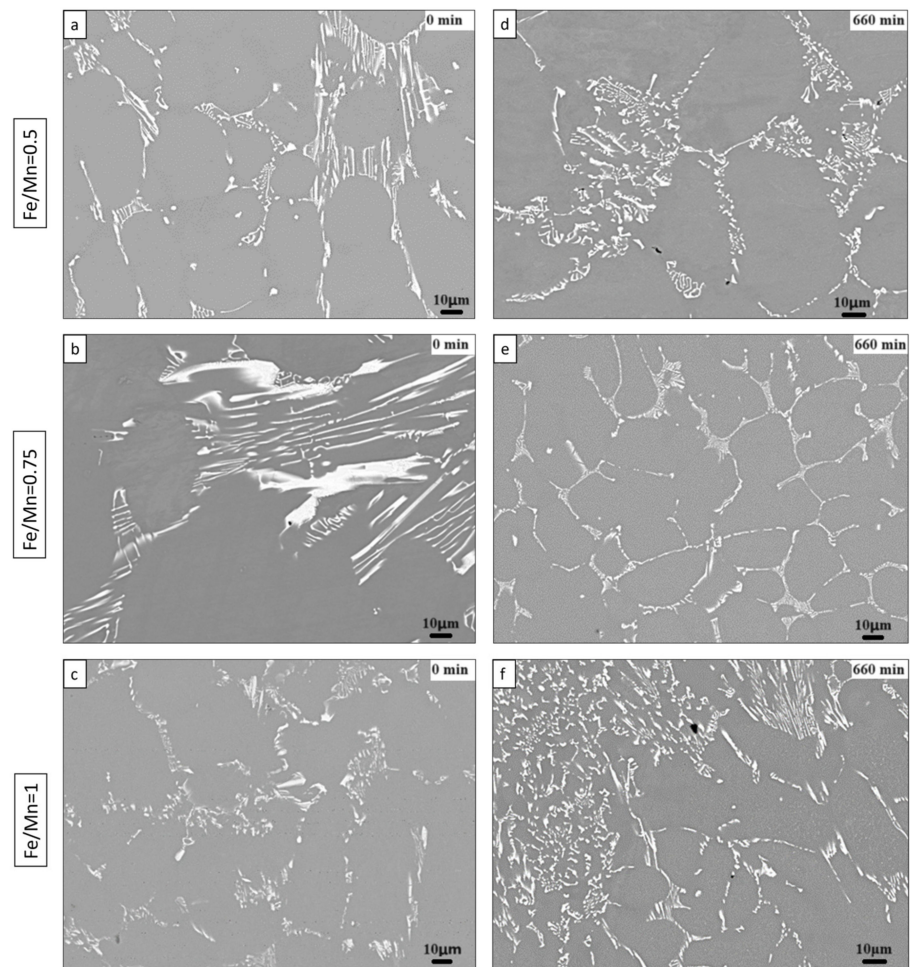
Figure 1. Micrographs of cast samples (**a**–**c**) and homogenized samples (**d**–**f**) taken at 500× magnification.

3.1.1. Fe/Mn = 0.5 Ratio

Figure 2 displays a micrograph at 5000× of the cast sample, comprising a porous light gray phase and a dark gray phase. Figure 3 illustrates the mapping of these phases at 5000×, revealing that the light phase contains Al, Fe, Mn, and Si, while the dark phase contains Al, Fe, and Mn only. The morphology of the microstructure exhibits irregular polygonal holes for the light phase and irregular polygonal shapes for the dark phase. Further analysis, quantification, and mapping confirm that the intermetallics present are Al_6FeMn and $Al_{15}(FeMn)_3Si_2$. As in the previous ratios, these intermetallics are Al_6FeMn and $Al_{15}(FeMn)_3Si_2$. This ratio has the highest amount of manganese among the three used, which means the Al_6FeMn phase for this ratio has the highest amount of manganese in the quantitative analyses.
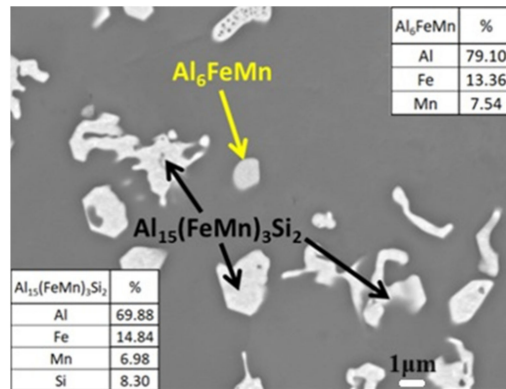
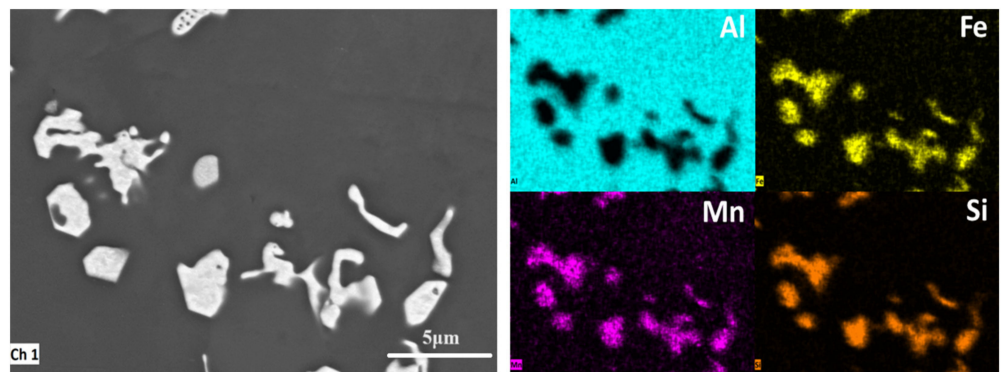**Figure 2.** SEM micrograph of a cast sample with an Fe/Mn ratio of 0.5.

Figure 3. Elemental mapping using EDS on a cast sample with an Fe/Mn ratio of 0.5.

Figures 4 and 5 display a micrograph and mapping at $2500\times$ of the sample that underwent 660 min of homogenization heat treatment from the Fe/Mn = 0.5 ratio. The mapping carried out shows only one intermetallic in the analyzed area. The light gray phase observed in the mapping analysis contains the following elements: Al, Fe, Mn, and Si. Based on the mapping, punctual analysis, and quantification results, it can be concluded that this intermetallic is $Al_{15}(FeMn)_3Si_2$.
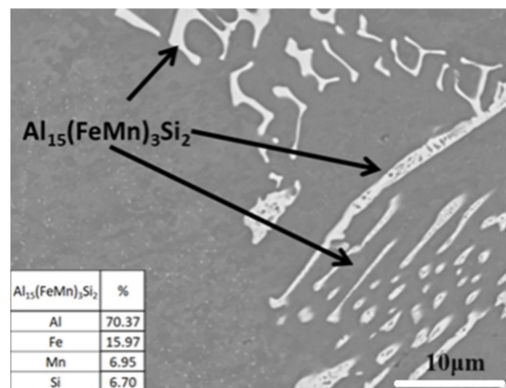

Figure 4. SEM micrograph of a sample homogenized for 660 min, with an Fe/Mn ratio of 0.5.
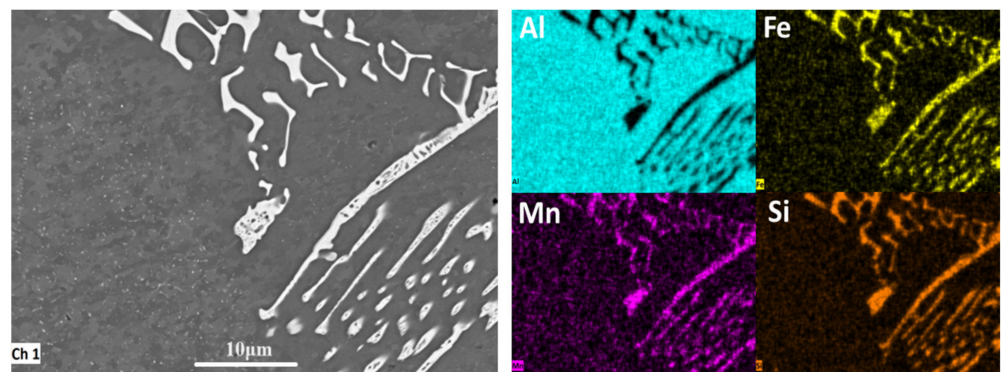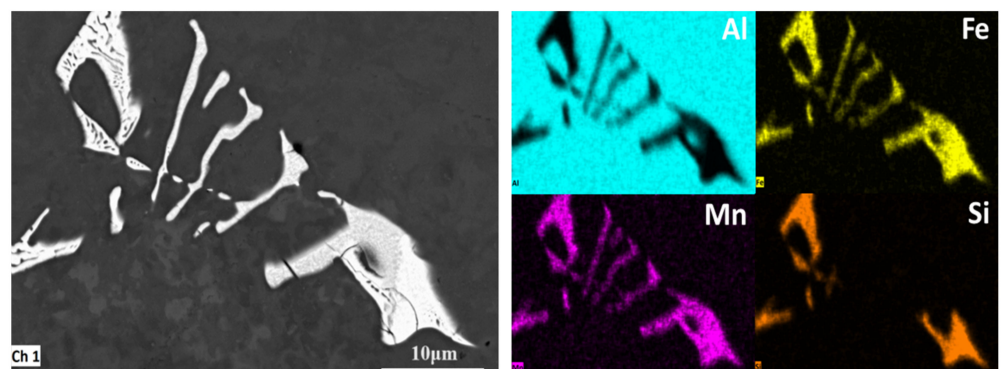
Figure 5. Elemental mapping using EDS on a sample homogenized for 660 min, with an Fe/Mn ratio of 0.5.

3.1.2. Fe/Mn = 0.75 Ratio

The micrograph in Figure 6, taken at 2500× magnification, displays two intermetallic compounds. One appears light gray and porous, while the other appears shadow gray and contains only Al, Fe, and Mn. The elemental mapping in Figure 7, also at 2500×, reveals that the light phase includes the following elements: Al, Fe, Mn, and Si. On the other hand, the dark gray phase shows Al, Fe, and Mn. These intermetallic compounds are identified as Al_6FeMn and $Al_{15}(FeMn)_3Si_2$.
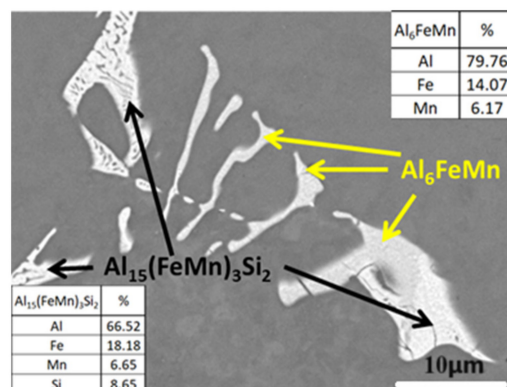
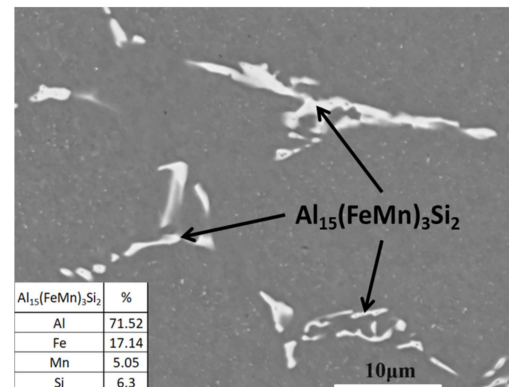**Figure 6.** SEM micrograph of a cast sample with an Fe/Mn ratio of 0.75.

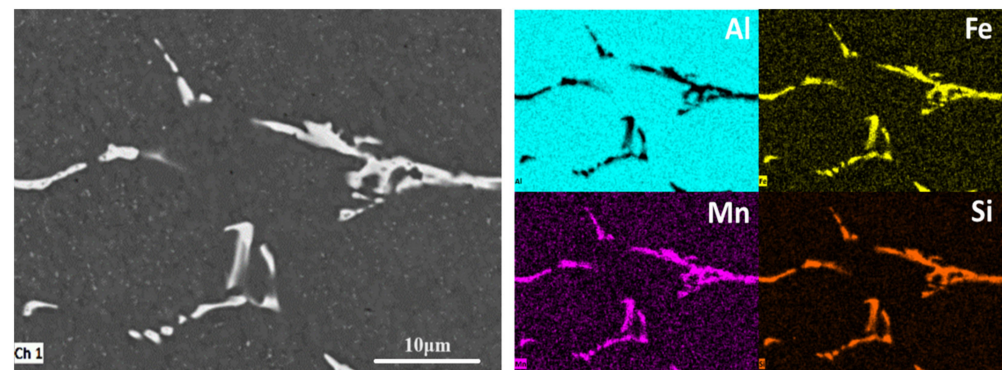**Figure 7.** Elemental mapping using EDS on a cast sample with an Fe/Mn ratio of 0.75.

It should be noted that these phases were also observed in an Fe/Mn ratio of 1, but the amount of Mn in the Al_6FeMn compound was found to be 2% higher compared to the Fe/Mn = 1 ratio.

Figures 8 and 9 show a micrograph and map at 2500× of a sample that underwent 660 min of homogenization heat treatment. The map indicates the presence of a single

intermetallic in the analyzed area, with a light phase showcasing the elements Al, Fe, Mn, and Si. Further analysis revealed that this phase is $Al_{15}(FeMn)_3Si_2$. However, due to the homogenization heat treatment, the shape of the phase changed from an irregular polygon with holes to a Chinese-script morphology. A light gray phase is visible in both figures, with elemental mapping confirming the presence of Al, Fe, Mn, and Si. Based on the point analysis and quantification, this phase is identified as $Al_{15}(FeMn)_3Si_2$. The heat treatment resulted in changes in the casting structure's morphology, transforming it from an irregular polygon with holes to a Chinese-script morphology.

Figure 8. SEM micrograph of a sample homogenized for 660 min with an Fe/Mn ratio of 0.75.

Figure 9. Elemental mapping using EDS on a sample homogenized for 660 min with an Fe/Mn ratio of 0.75.

3.1.3. Fe/Mn = 1 Ratio

Figures 10 and 11 display mappings and micrographs of cast samples obtained from Fe/Mn = 1 ratio. The figures show two different phases of particles. The mapping shows two phases present in the analyzed zone, represented with different colors. The light gray phase contains elements such as Al, Fe, Mn, and Si, while the dark gray phase contains Al, Fe, and Mn. Both phases are irregular polygons in morphology. The punctual analysis, quantification, and mapping concluded that the phases correspond to the Al_6FeMn and $Al_{15}(FeMn)_3Si_2$ intermetallics.
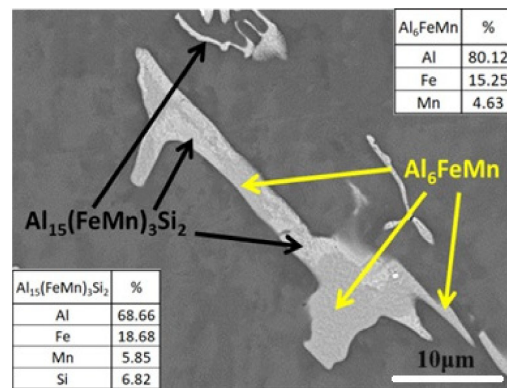
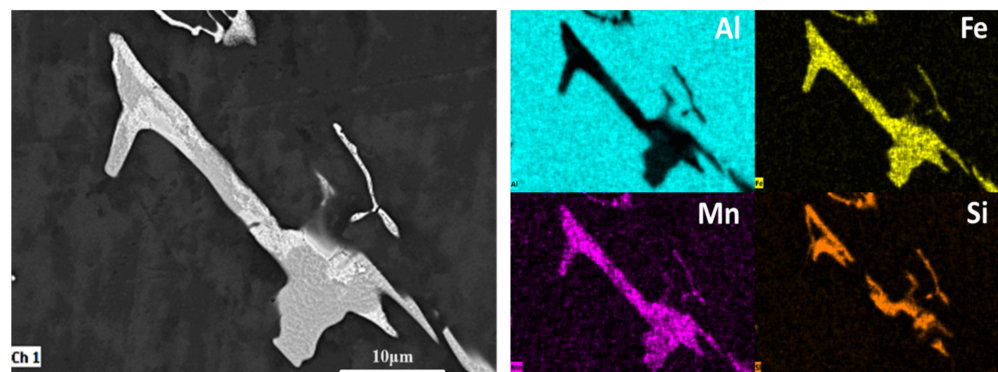**Figure 10.** SEM micrograph of a cast sample with an Fe/Mn ratio of 1.

Figure 11. Elemental mapping using EDS on a cast sample with an Fe/Mn ratio of 1.

Figures 12 and 13 show the heat treatment results on Fe/Mn = 1 ratio alloy samples for 660 min. The micrograph at 2500× magnification depicts a light gray phase that contains Al, Fe, Mn, and Si elements. Based on the mapping results, analysis, and quantification, it was determined that the phase was $Al_{15}(FeMn)_3Si_2$. The sample's morphology changed to irregular polygonal shapes with holes compared to the cast sample. The main objective of the heat treatment was to transform the Al_6FeMn phase into the $Al_{15}(FeMn)_3Si_2$ cubic phase.
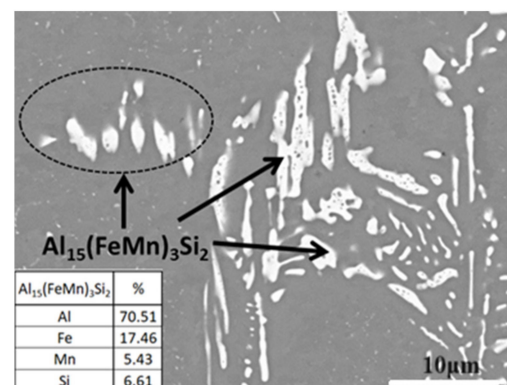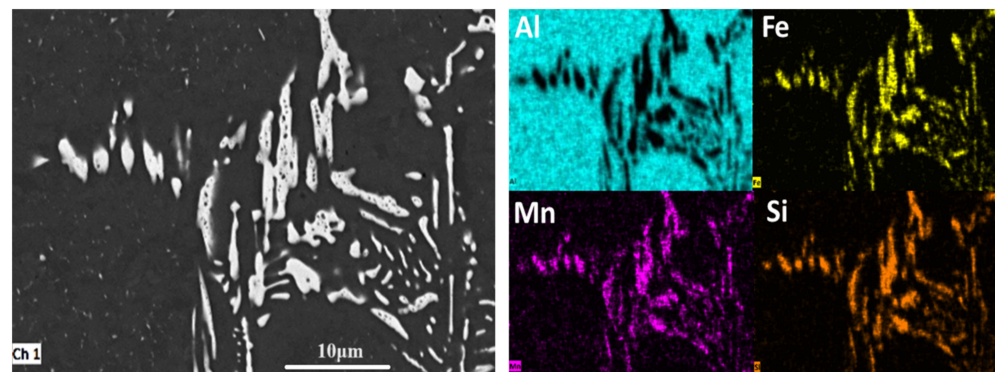

Figure 12. SEM micrograph of a sample homogenized for 660 min with an Fe/Mn ratio of 1.

Figure 13. Elemental mapping using EDS on a sample homogenized for 660 min with an Fe/Mn ratio of 1.

In each of the micrographs presented for the Fe/Mn ratios of 0.5, 0.75, and 1, the changes in morphology and transformation of phases are a result of the homogenization heat treatment. The presence of the $Al_{15}(FeMn)_3Si_2$ phase in the casting microstructure can be attributed to manganese, which acts as a catalyst and accelerates the reaction to promote the formation of the $Al_{15}(FeMn)_3Si_2$ phase.

The microstructures show an increased volume fraction of the phase with Chinese-script and irregular polygon morphology in the Fe/Mn = 0.5 ratio after 660 min of heat treatment compared to the other ratios. This phase also occurs at shorter times, which can be attributed to the fact that the amount of manganese in this ratio is twice as much as that of iron.

It has been observed that for the Fe/Mn ratios of 1 and 0.75, the same pattern is seen in the casting structure containing both the β and α phases, while an increase in heat treatment time leads to a rise in the α phase and a decrease in the β phase.

Based on the results obtained, it can be concluded that the casting microstructure contains $β\text{-}Al_6FeMn$ and $α\text{-}Al_{15}(FeMn)_3Si_2$ phases with an irregular polygon morphology. However, after subjecting the samples to homogenization heat treatment for 660 min, only the $α\text{-}Al_{15}(FeMn)_3Si_2$ phase with Chinese-script and holes of irregular polygon morphology was observed. This suggests that homogenization heat treatment transformed the $β\text{-}Al_6FeMn$ phase obtained from casting into the $α\text{-}Al_{15}(FeMn)_3Si_2$ phase. This transformation occurred through the diffusion of silicon in the β phase and, subsequently, nucleation and growth of the α phase.

The literature reports the mechanism of α phase transformation, which starts with nucleation of $α\text{-}Al_{15(}FeMn)_3Si_2$ at particle–matrix interfaces, grows through the particles, and invades the Al_6FeMn phase [23,24].

The growth process can be identified as a eutectoid process, where the Al_6FeMn phase decomposes into a mixture of α-phase and an aluminum solid solution. The nucleation process controls the rate of the overall transformation, as the growth of the α-phase is rapid. The transformation from β to α is dependent on the diffusion of silicon from the matrix into the particles, thus making silicon an important factor in this process [25,26].

The quaternary intermetallic compound AlFeMnSi has a stoichiometry that is defined based on its chemical composition. For an Fe/Mn ratio of 1, the stoichiometry is $Al_8FeMnSi_2$. For an Fe/Mn ratio of 0.99, the stoichiometry is $Al_{0.66}Fe_{0.081}Mn0._{082}Si_{0.175}$. For an Fe/Mn ratio of 0.63, the stoichiometry is $Al_{11.8}FeMn_{1.6}Si_{1.6}$. Finally, for an Fe/Mn ratio of 0.25, the stoichiometry is $Al_{16}(FeMn)_4Si_3$ [27]. A previous study found an acicular morphology $α\text{-}Al_{12}(FeMn)_3Si$ phase with an fcc structure. In another study, with alloy 6016, the chemical composition was modified by increasing the Fe and Mn contents (1.4% Fe and 1.1% Mn), and the morphology reported was the Chinese-script with a cubic structure, as discovered by EDS analyses, and thermodynamic simulations indicated that it could be the $α\text{-}AlFeSi$ or the $α\text{-}Al(FeMn)Si$ phase [28].

3.2. Analysis of the β and α Phases by X-ray Diffraction

The results of the analysis to identify the phases present in the casting samples were corroborated through X-ray diffraction, as scanning electron microscopy had been previously used. The analysis was performed on samples with different Fe/Mn ratios before and after a 660 min homogenization heat treatment. Figure 14 displays the diffraction patterns for each of the ratios.
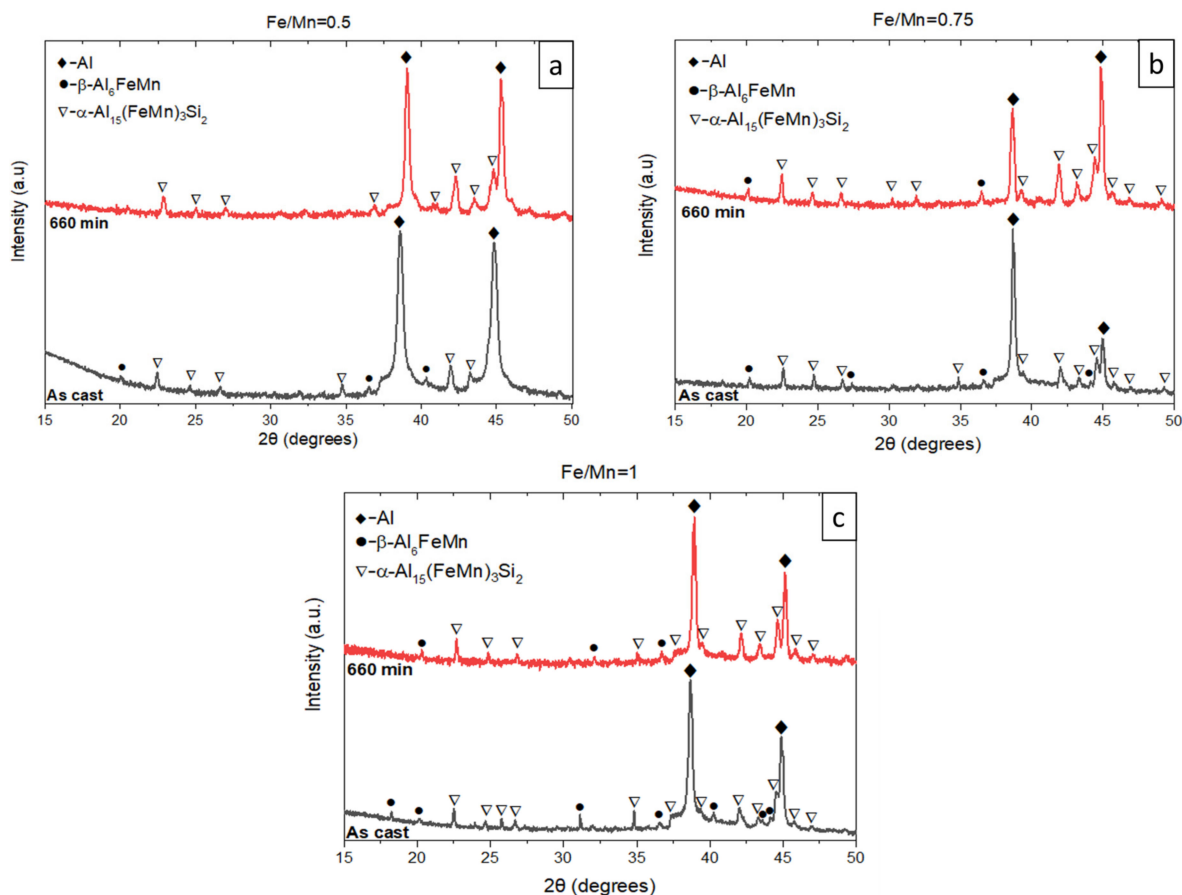
Figure 14. X-ray diffraction patterns with different Fe/Mn ratios: (**a**) 0.5, (**b**) 0.75, and (**c**) 1.

The analysis revealed the presence of an aluminum matrix and two phases: β-Al_6FeMn and α-$Al_{15}(FeMn)_3Si_2$. These phases were observed in the casting samples, but only the α-$Al_{15}(FeMn)_3Si_2$ phase was present after the homogenization heat treatment. This was because the β-Al_6FeMn phase had precipitated in the casting structure and was fully converted into the α-$Al_{15}(FeMn)_3Si_2$ phase after the heat treatment.

For the Fe/Mn = 0.5 ratio, only the α-$Al_{15}(FeMn)_3Si_2$ phase was present, which can be attributed to the higher manganese content in this ratio. The addition of manganese promoted the formation of this phase. In contrast, for the Fe/Mn = 1 and 0.75 ratios, the β-Al_6FeMn phase was present even after the heat treatment but in reduced proportions. The objective of the heat treatment was to transform the β-Al_6FeMn phase into the α-$Al_{15}(FeMn)_3Si_2$ phase, and this was achieved to a greater extent in the Fe/Mn = 0.5 ratio due to the higher amount of manganese.

Overall, this study concludes that the presence of the β-Al_6FeMn and α-$Al_{15}(FeMn)_3Si_2$ phases can be observed in the casting samples, but the homogenization heat treatment can transform the former into the latter phase, especially when the manganese content is high.

The X-ray diffraction results identified the presence of the α-$Al_{15}(FeMn)_3Si_2$ phase, this validates the information obtained in the SEM analyses, in which the morphology of this phase was observed to be divided into massive and regular polyhedrons, hollow and

regular polyhedrons, and multi-branched polyhedrons. The results of X-ray diffraction, and the morphology for the α-$Al_{15}(FeMn)_3Si_2$ phase of this study, are consistent with a previous report, where similar morphologies and regular polyhedrons, hollow and regular polyhedrons, and multi-branched polyhedrons for the α-$Al_{15}(FeMn)_3Si_2$ phase were found [29]. Additionally, the α-$Al_{15}(FeMn)_3Si_2$ phase was found to have several morphologies, including polygon + thick Chinese-script, dense Chinese-script + polygon, and polygonal + dense Chinese-script [30]. Table 4 shows the crystallographic information of the analyzed phases.

Table 4. Crystallographic information of the analyzed phases.

Phase	Crystal System	Stoichiometry	Space Group	Cell Parameters
β-AlFeMn	Orthorhombic	Al_6FeMn	C m c m (63)	a = 7.49800 Å b = 6.49500 Å c = 8.83700 Å
α-Al(FeMn)Si	Cubic	$Al_{15}(FeMn)_3Si_2$	P m-3 (200)	a = 12.5600 Å

3.3. Quantification of β-Al_6FeMn and α-$Al_{15}(FeMn)_3Si_2$ Phases

During phase quantification, thirteen samples underwent analysis for each Fe/Mn ratio. To examine the microstructure, optical microscopy images were captured at 1000× magnification, revealing both β and α phases in all samples with Fe/Mn ratios of 0.5, 0.75, and 1. The casting structure displayed consistent microstructural characteristics across all three ratios, with the phases being evident.

Through the analysis of the β and α phases, an area of approximately 5% was determined. To ensure utmost precision, the percentages of each phase were evaluated in ten different fields. The micrographs of the casting samples at Fe/Mn ratios of 0.5, 0.75, and 1 confirm the presence of the α phase, which was then named casting alpha. The corresponding casting α phase percentages for Fe/Mn ratios of 0.5, 0.75, and 1 were obtained from the casting sample and found to be 2.31%, 2.08%, and 2.10% of the area for this phase and the area of the β phase was 2.69%, 2.92% and 2.90% for Fe/Mn ratios of 0.5, 0.75, and 1, respectively; these values are considered as the initial amount of this phase, from which the percentage of transformation to α phase is determined.

The analysis of the $\beta \rightarrow \alpha$ transformation involved setting the percentage of the casting α phase to zero, which allowed for the determination of the percentage of the β phase. Micrographs of samples attacked with Keller reagent for the quantification of the β and α phases are presented in Figure 15. The distinct color tones of the phases in the micrographs are a result of a chemical attack with the Keller reagent. This approach enabled the quantification of each phase in the analyzed sample using Image-Pro 6.0 software.

The transformed fraction (θ) changes as the reaction takes place, until the reagents are transformed into products. In a reaction, the value of (θ) can be calculated from the reduction of the area of the compound intermetallic β to time (t), related to the total decrease in area, which corresponds to the end of the reaction. The transformed fraction (θ) is determined using Equation (1):

$$(\theta) = \frac{\theta_1}{\theta_0 + \beta_0} * 100 \tag{1}$$

where θ_0 is the initial transformed fraction of phase α, θ_1 is the percentage of phase α transformed at time t, and β_0 is the percentage of phase β [31].
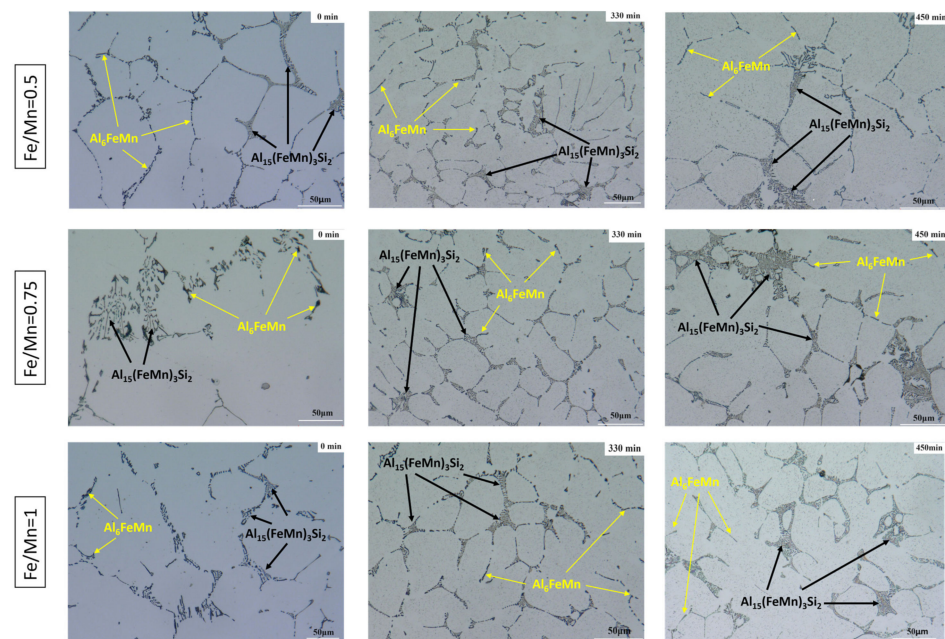
Figure 15. Micrographs of samples attacked with Keller reagent for the quantification of the β and α phases.

Table 5 displays the percentage of the transformed fraction obtained for both inter-metallics β and α in each heat treatment condition.

Table 5. Results of the quantification for the percentages of the transformed fraction β and α phases.

Time	Ratio					
	Fe/Mn = 0.5		Fe/Mn = 0.75		Fe/Mn = 1	
Min	β (%)	α (%)	β (%)	α (%)	β (%)	α (%)
As cast	2.69	0	2.92	0	2.90	0
120	2.19	0.50	2.32	0.60	2.58	0.32
210	1.99	0.70	2.17	0.75	2.37	0.53
240	1.83	0.86	2.10	0.82	2.31	0.59
270	1.75	0.94	2.02	0.90	2.23	0.67
300	1.64	1.05	1.89	1.03	2.10	0.80
330	1.53	1.16	1.79	1.13	2.09	0.81
360	1.3	1.39	1.71	1.21	1.92	0.98
390	1.15	1.54	1.65	1.27	1.81	1.09
420	0.98	1.71	1.4	1.52	1.70	1.20
450	0.76	1.93	1.12	1.80	1.62	1.28
540	0	2.69	0.72	2.20	1.32	1.58
660	0	2.69	0.4	2.52	0.81	2.09
Total (%)	0	100	14	86	28	72

According to the findings, the longer the heat treatment time, the more the β phase converts to the α phase. This is due to an increase in the α phase fraction and a decrease in the β phase fraction, which begins at the 120 min mark for all three ratios. Initially, the β phase fraction is comparable among the three ratios, ranging from 2.69 to 2.92. Notably, the Fe/Mn = 0.5 ratio achieved a complete transformation from β to α phase in 540 min, which

was faster than the other ratios. Figure 16 displays the percentages of β and α phases for different ratios with homogenization heat treatment at 575 °C.
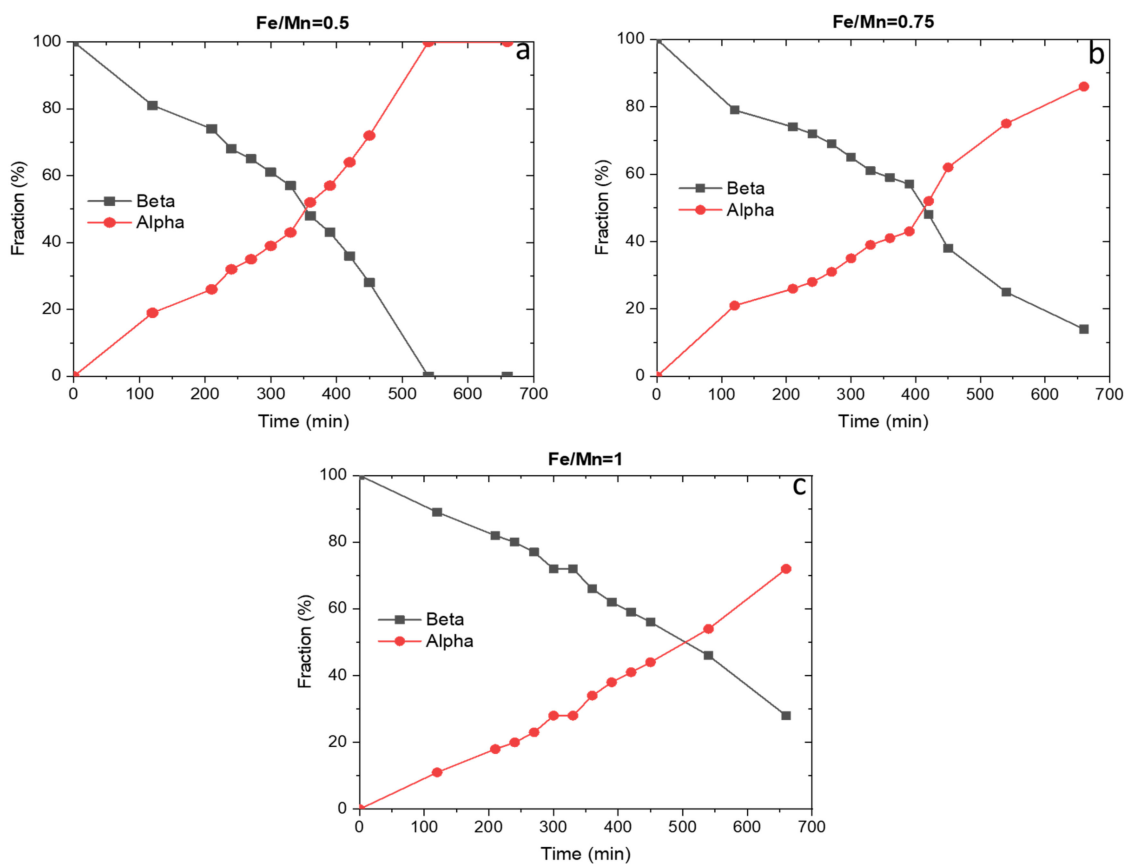
Figure 16. Percentage of β and α phase for Fe/Mn ratios: (**a**) 0.5, (**b**) 0.75, and (**c**) 1, with homogenization heat treatment at 575 °C.

The results of the quantification of the α and β phases indicate that the variations in the chemical composition of the elements, in this case, Fe and Mn for each of the analyzed ratios, result in both β and α phases being present in the casting microstructure; the formation of an α phase from casting has a great impact so that the β→α transformation is carried out in very short times when subjecting them to the homogenization thermal treatment. This transformation occurred through the diffusion of silicon in the β phase and, subsequently, nucleation of α-Al$_{15}$(FeMn)$_3$Si$_2$ at particle–matrix interfaces, growing through the particles and invading the Al$_6$FeMn phase.

4. Conclusions

The use of Fe/Mn ratios has been found to prevent the formation of needle-shaped β-Al$_5$FeSi in the casting structure of the alloy. Instead, it encourages the precipitation of β-Al$_6$FeMn and α-Al$_{15}$(FeMn)$_3$Si$_2$ phases. The presence of these phases improves the mechanical properties of the alloy as the α-type intermetallic is characterized by ductility, which provides the material with easy deformation. The casting structure's formation of these β-Al$_6$FeMn and α-Al$_{15}$(FeMn)3Si$_2$ phases is attributed to the manganese, which acts as a catalyst.

The presence of manganese as a catalyst speeds up the formation of the Al$_{15}$(FeMn)$_3$Si$_2$ phase reaction during the heat treatment process of homogenization. Manganese diffuses through the alloy, reducing the diffusion time and leading to the nucleation and growth of the β-Al$_6$FeMn phase. This phase is already present in the casting structure due to the quantity of iron and manganese used.

During the heat treatment process of homogenization, the β-Al$_6$FeMn phase obtained during casting is transformed to the α-Al$_{15}$(FeMn)$_3$Si$_2$ phase. This transformation happens due to silicon diffusion in the β phase, which results in the nucleation of the α phase at the particle–matrix interfaces. The growth of the α phase then occurs through the particles, replacing the Al$_6$FeMn phase.

The mapping-based elemental analysis revealed that the cast and heat-treated samples have α phases that contain Al, Fe, Si, and Mn, and β phases that contain Al, Fe, and Mn elements. X-ray diffraction confirmed that these phases correspond to the β-Al$_6$FeMn and α-Al$_{15}$(FeMn)$_3$Si$_2$ phases.

References

1. Yan, L.Z.; Zhang, Y.G.; Li, X.W.; Li, Z.H.; Wang, F.; Liu, H.W.; Xiong, B.Q. Investigation of the microstructure evolution of 6016 aluminum alloy during homogenization. *Adv. Mater. Res.* **2013**, *668*, 784–788. [CrossRef]
2. Singh, P.; Ramacharyulu, D.A.; Kumar, N.; Saxena, K.K.; Eldin, S.M. Change in the structure and mechanical properties of Al-Mg-Si alloys caused by the addition of other elements: A comprehensive review. *J. Mater. Res. Technol.* **2023**, *27*, 1764–1796. [CrossRef]
3. Whalen, S.; Overman, N.; Taysom, B.S.; Bowden, M.; Reza-E-Rabby, M.; Skszek, T.; DiCiano, M. Effect of high iron content on direct recycling of unhomogenized aluminum 6063 scrap by Shear Assisted Processing and Extrusion. *J. Manuf. Process.* **2023**, *97*, 115–124. [CrossRef]
4. Puncreobutr, C.; Phillion, A.; Fife, J.; Rockett, P.; Horsfield, A.; Lee, P. In situ quantification of the nucleation and growth of Fe-rich intermetallics during Al alloy solidification. *Acta Mater.* **2014**, *79*, 292–303. [CrossRef]
5. Medvecká, D.; Kucharíková, L.; Uhríčik, M. The failure degradation of recycled aluminum alloys with high content of β-Al5FeSi intermetallic phases. *Trans. Tech. Publ.* **2020**, *403*, 97–102.
6. Alvarez-Antolin, F.; Asensio-Lozano, J.; Cofiño-Villar, A.; Gonzalez Pociño, A. Analysis of different solution treatments in the transformation of β-AlFeSi particles into α-(FeMn)Si and their Influence on different ageing treatments in Al-Mg-Si alloys. *Metall. J.* **2020**, *10*, 620. [CrossRef]
7. Wang, X.; Ma, P.-K.; Zhang, S.-Y.; Liu, X.; Wang, C.; Wang, D.-W.; Wang, H.-Y. High-ductility AA6061 alloys produced by combination of sub-rapid solidification and Cr-alloying. *J. Mater. Res. Technol.* **2022**, *18*, 1566–1577. [CrossRef]
8. Liu, X.; Wang, C.; Zhang, S.-Y.; Song, J.-W.; Zhou, X.-L.; Zha, M.; Wang, H.-Y. Fe-bearing phase formation, microstructure evolution, and mechanical properties of Al-Mg-Si-Fe alloy fabricated by the twin-roll casting process. *J. Alloys Compd.* **2021**, *886*, 161202. [CrossRef]
9. Katsivarda, M.; Vazdirvanidis, A.; Pantazopoulos, G.; Kolioubas, N.; Papadopoulou, S.; Rikos, A.; Spiropoulou, E.; Papaefthymiou, S. Investigation of the effect of homogenization practice of 6063 alloy billets on beta to alpha transformation and of the effect of cooling rate on precipitation kinetics. *Mater. Sci. Forum* **2018**, *941*, 884–889. [CrossRef]
10. Uttarasak, K.; Chongchitnan, W.; Matsuda, K.; Chairuangsri, T.; Kajornchaiyakul, J.; Banjongprasert, C. Evolution of Fe-containing intermetallic phases and abnormal grain growth in 6063 aluminum alloy during homogenization. *Results Phys.* **2019**, *15*, 102535. [CrossRef]
11. Bayat, N.; Carlberg, T.; Cieslar, M. In-situ study of phase transformations during homogenization of 6005 and 6082 Al alloys. *J. Alloys Compd.* **2017**, *725*, 504–509. [CrossRef]
12. Liu, C.L.; Azizi-Alizamini, H.; Parson, N.C.; Poole, W.J.; Du, Q. Microstructure evolution during homogenization of Al-Mg-Si-Mn-Fe alloys: Modelling and experimental results. *Trans. Nonferrous Met. Soc. China* **2017**, *27*, 747–753. [CrossRef]

13. Kemsies, R.H.; Milkereit, B.; Wenner, S.; Holmestad, R.; Kessler, O. In situ DSC investigation into the kinetics and microstructure of dispersoid formation in Al-Mn-Fe-Si(-Mg) alloys. *Mater. Des.* **2018**, *146*, 96–107. [CrossRef]

14. Warmuzek, M. Solidification path of the AlFeMnSi alloys in a stage of primary intermetallic phases precipitation. *Trans. Foundry Res. Inst.* **2015**, *55*, 51–60.

15. Gao, T.; Hu, K.; Wang, L.; Zhang, B.; Liu, X. Morphological evolution and strengthening behavior of α-Al(Fe,Mn)Si in Al–6Si–2Fe–xMn alloys. *Results Phys.* **2017**, *7*, 1051–1054. [CrossRef]

16. Österreicher, J.A.; Kumar, M.; Schiffl, A.; Schwarz, S.; Bourret, G.R. Secondary precipitation during homogenization of Al-Mg-Si alloys: Influence on high temperature flow stress. *Mater. Sci. Eng. A* **2017**, *687*, 175–180. [CrossRef]

17. Zhao, Q.; Qian, Z.; Cui, X.; Wu, Y.; Liu, X. Influences of Fe, Si and homogenization on electrical conductivity and mechanical properties of dilute Al-Mg-Si alloy. *J. Alloys Compd.* **2016**, *666*, 50–57. [CrossRef]

18. Liu, X.; Jia, H.L.; Wang, C.; Wu, X.; Zha, M.; Wang, H.Y. Enhancing mechanical properties of twin-roll cast Al–Mg–Si–Fe alloys by regulating Fe-bearing phases and macro-segregation. *Mater. Sci. Eng. A* **2022**, *831*, 142256. [CrossRef]

19. Baldan, R.; Malavazi, J.; Couto, A. Microstructure and mechanical behavior of Al9Si0.8Fe alloy with different Mn contents. *Mater. Sci. Technol.* **2017**, *33*, 1192–1199. [CrossRef]

20. Rosefort, M.; Matthies, C.; Buck, H.; Koch, H. Using SEM and EDX for a simple differentiation of α- and β-AlFeSi-Phases in Wrought Aluminum Billets. In *Light Metals 2011: The Minerals*; Lindsay, S.J., Ed.; Metals & Materials Society: Pittsburgh, PA, USA, 2011; pp. 711–716.

21. Liu, F.; Zhu, X.; Qin, J.; Zhou, W.; Ling, J.; Dong, Q.; Yu, J.; Nagaumi, H.; Zhang, B. Effect of Mn/Cr ratio on precipitation behaviors of α-Al(FeMnCr)Si dispersoids and mechanical properties of Al–Mg–Si–Cu alloys. *Mater. Sci. Eng. A* **2022**, *860*, 144269. [CrossRef]

22. Liu, X.; Ma, Y.-L.; Wang, X.; Zhang, S.-Y.; Zhang, M.-X.; Wang, H.-Y. Enhanced long-term thermal stability and mechanical properties of twin-roll cast Al–Mg–Si alloys with Mn and Cu additions. *Mater. Sci. Eng. A* **2023**, *872*, 144945. [CrossRef]

23. Alexander, D.T.L.; Greer, A.L. Nucleation of the Al6(Fe,Mn)- to-α-Al–(Fe,Mn)–Si transformation in 3XXX aluminium alloys. I. Roll-bonded diffusion couples. *Philos. Mag.* **2004**, *84*, 3051–3070. [CrossRef]

24. Trømborg, E.; Dons, A.L.; In, L.A.; Lohne, O.; Nes, E.; Ryum, N. (Eds.) *Aluminium Alloys: Their Physical and Mechanical Properties: ICAA3*; SINTEF Metallurgy: Trondheimin, Norway, 1992; pp. 270–275.

25. Alexander, D.; Greer, A. Solid-state intermetallic phase tranformations in 3XXX aluminium alloys. *Acta Mater.* **2002**, *50*, 2571–2583. [CrossRef]

26. Anyalebechi, P.N. Effects of silicon, iron, and chromium on the response of aluminum alloy 3004 ingots to homogenization. In Proceedings of the TMS Annual Meeting, New Orleans, LA, USA, 9–13 March 2008; pp. 201–218.

27. Qian, X.; Parson, N.; Chen, X.G. Effect of homogenization treatment and microalloying with Mn on the microstructure and hot workability of AA6060 aluminum alloys. *J. Mater. Eng. Perform.* **2019**, *28*, 4531–4542. [CrossRef]

28. Trink, B.; Weißensteiner, I.; Uggowitzer, P.J.; Strobel, K.; Pogatscher, S. High Fe content in Al-Mg-Si wrought alloys facilitates excellent mechanical properties. *Scr. Mater.* **2022**, *215*, 114701. [CrossRef]

29. Song, D.F.; Zhao, Y.L.; Wang, Z.; Jia, Y.-W.; Li, D.-X.; Fu, Y.-N.; Zhang, D.-T.; Zhang, W.-W. 3D Fe-Rich Phases Evolution and Its Effects on the Fracture Behavior of Al–7.0Si–1.2Fe Alloys by Mn Neutralization. *Acta Metall. Sin.* **2022**, *35*, 163–175. [CrossRef]

30. Song, D.F.; Jia, Y.; Li, Q.; Zhao, Y.; Zhang, W. Effect of Initial Fe Content on Microstructure and Mechanical Properties of Recycled Al-7.0Si-Fe-Mn Alloys with Constant Mn/Fe Ratio. *Materials* **2022**, *15*, 1618. [CrossRef]

31. Aguilar, I.G.; Torres, J.T.; Valdés, A.F.; Saldivar, A.A.F. The effect of interrumped homogenization on β-Al5FeMnSi→α-Alx(Fe and Mn)Si transformation in the A6063 aluminum alloy. *Metals* **2022**, *12*, 2117. [CrossRef]